Comparison of 10 Multi-Sensor Image Fusion Paradigms for IKONOS Images

Uttam Kumar[1, 2], Anindita Dasgupta[3], Chiranjit Mukhopadhyay[1], N. V. Joshi[3], and T. V. Ramachandra[2, 3, 4]

[1]Department of Management Studies, [2]Centre for Sustainable Technologies,
[3]Centre for Ecological Sciences, [4]Centre for *infrastructure*, Sustainable Transport and Urban Planning,
Indian Institute of Science, Bangalore -560012, India

Abstract: Fusion of multi-sensor imaging data enables a synergetic interpretation of complementary information obtained by sensors of different spectral ranges. Multi-sensor data of diverse spectral, spatial and temporal resolutions require advanced numerical techniques for analysis and interpretation. This paper reviews ten advanced pixel based image fusion techniques – Component substitution (COS), Local mean and variance matching, Modified IHS (Intensity Hue Saturation), Fast Fourier Transformed-enhanced IHS, Laplacian Pyramid, Local regression, Smoothing filter (SF), Sparkle, SVHC and Synthetic Variable Ratio. The above techniques were tested on IKONOS data (Panchromatic band at 1 m spatial resolution and Multispectral 4 bands at 4 m spatial resolution). Evaluation of the fused results through various accuracy measures, revealed that SF and COS methods produce images closest to corresponding multi-sensor would observe at the highest resolution level (1 m).

Keywords: image fusion, multi-sensor; multi-spectral, IKONOS

NOMENCLATURE

PAN	Panchromatic
MS	Multi-spectral
HSR	High spatial resolution
LSR	Low spatial resolution
COS	Component Substitution
LMVM	Local Mean and Variance Matching
IHS	Intensity Hue Saturation
FFT	Fast Fourier Transform
LP	Low Pass
HP	High Pass
SF	Smoothing Filter
GLP	Generalised Laplacian Pyramid
LR	Local Regression
SVHC	Simulateur de la Vision Humaine des Couleurs
SVR	Synthetic Variable Ratio
CC	Correlation Coefficient
UIQI	Universal Image Quality Index
R-G-B	Red-Green-Blue
NIR	Near Infra Red
FCC	False colour composite
BT	Brovey Transform
HPF	High Pass Filtering
HPM	High Pass Modulation
PCA	Principal Component Analysis
ATW	À Trous Algorithm-Based Wavelet Transform
MRAIM	Multiresolution Analysis-Based Intensity Modulation
GS	Gram Schmidt
LMM	Local Mean Matching
IRS	Indian Remote Sensing Satellite
MRA	Modulation and Multi-resolution Analysis
UNB	University of New Brunswick

1. Introduction

Images acquired from space borne Earth observation satellites such as QuickBird, IKONOS, IRS bundle 1:4 ratio of a high spatial resolution (HSR) Panchromatic (PAN) band and low spatial resolution (LSR) Multi-spectral (MS) bands in order to support both spectral and best spatial resolutions while minimising on-board data handling needs [1]. Fusion of multi-sensor data enhances object delineation and interpretation due to integration of spatial information from HSR PAN and spectral information from LSR MS images. For example, fusion of 1m IKONOS PAN image with 4 m MS images allow identification of objects approximately one meter in length on the Earth's surface, especially useful in urban areas, because the characteristic of urban objects are determined not only by their spectra but also by their structure. This objective of this paper is to perform a comparative analysis of ten advanced pixel based image fusion techniques on IKONOS PAN and MS data.

2. Image Fusion Techniques

Images are radiometrically and geometrically corrected (at pixel level) and geo-registered considering the topographic undulations. For all methods discussed here (except generalised Laplacian pyramid), it is assumed that LSR MS images are upsampled to the size of HSR PAN image.

2.1. Component Substitution (COS) – A set of LSR M-bands MS data (MS_{LOW}) and a HSR PAN data (PAN_{HIGH}) fusion using COS method involves three steps:

1) Transforming the MS data from spectral space to some other feature space by linear transformations.
2) Substituting one component with the HSR data derived from PAN.
3) Transforming the transformed band back to the spectral space to get HSR MS data. The fused MS image is given by:

$$MS_{HIGH} = MS_{LOW} + \overline{W}\delta \quad (1)$$

where, MS_{HIGH} is the fused image, $\overline{W}$ is the modulation coefficient, δ is the spatial detail of redundant information I,

$$\delta = (I^h - I^l) - E(I^h - I^l), \qquad I^h = rPAN_{HIGH},$$

$I^l = \overline{C}MS_{LOW}$ and $\overline{W}.\overline{C} = 1$. $E = (.)$ is the expectation of $(I^h - I^l)$. First, a linear regression of MS and PAN sensor SRF (spectral response function) is carried out. The regression coefficient $\overline{C}$ is obtained for each MS band. Next, the area of the part covered by both (intersection) of PAN SRF (denoted by S_{PAN}) and SRF of all the pooled MS bands (denoted as S_{inter}) are calculated. Ratio of S_{inter} and S_{PAN} is calculated (denoted by r), for IKONOS. W is calculated by

$$\overline{W} = \frac{S_m}{\sum S_m C_m} \quad (2)$$

where $S = (S_m)$ is the area of the part covered by both (union) SRF of MS band m and PAN, and S_m implies how much information is recorded by both the MS band m while it is recorded by PAN sensor [2].

2.2. Local Mean and Variance Matching (LMVM) –
LMVM matches both the local mean and variance values of the PAN image with those of the original LSR spectral channel given by

$$MS_{i,j}^{FUSED} = \frac{\left(PAN_{i,j}^{HIGH} - \overline{PAN}_{i,j}^{HIGH}\right) sd\left(MS_{i,j}^{LOW}\right)_{(w,h)}}{sd\left(PAN_{i,j}^{LOW}\right)_{(w,h)}} + \overline{MS}_{i,j}^{LOW} \quad (3)$$

where, $MS_{i,j}^{FUSED}$ is the fused image, $PAN_{i,j}^{HIGH}$ and $MS_{i,j}^{LOW}$ are respectively, the HSR and LSR images at pixel coordinates i, j, $\overline{PAN}_{i,j}^{HIGH}(w,h)$, $\overline{MS}_{i,j}^{LOW}(w,h)$ are local means calculated inside the window of size (w, h), sd is the local standard deviation, and $\overline{MS}_{i,j}^{LOW}$ is the mean of the LSR image [3].

2.3. Modified IHS (Intensity Hue Saturation) –
Here the input intensity (PAN band) is modified so that it looks more like the intensity of the input MS bands. The steps are:

1) **Choose the β coefficients:** β coefficients represent the relative contributions of each portion of the electromagnetic spectrum to the PAN band. A regression analysis is performed on M bands vs. the PAN band. If the MS and PAN data come from the same sensor, a linear regression is sufficient to derive a good relationship between the two datasets otherwise it may be possible to improve by using higher-order terms.

2) **Choose the α coefficients:** The desired output is equally weighted toward Red (R), Green (G), and Blue (B). In such cases, the α coefficients are equal and

given by $\quad \alpha = \dfrac{\sum_m \beta_m \overline{MS}_m}{3\overline{PAN}}$. (4)

$\overline{MS}_m$ =average of band m; $\overline{PAN}$ =average of PAN band; β_j =coefficient for band m.

3) **Generate modulation ratio:** Apply an RGB-to-IHS transform on the three MS bands and generate intensity modification ratio (r_1),

$$r_1 = \frac{a_r d_r + a_g d_g + a_b d_b}{\sum_m \beta_m d_m} \quad (5)$$

where, a_r=numerator coefficient for red DN value, d_r=DN value of band used for red output, a_g=numerator coefficient for green DN value, d_g=DN value of band used for green output, a_b=numerator coefficient for blue DN value, d_b=DN value of band used for blue output, β_m=denominator coefficient for DN value of band m and d_m=DN value of band m.

4) **Reverse transformation:** Multiply the modification ratio r_1 by the PAN band. Transform the modified IHS data back to RGB space to generate the final product using the modified intensity [4].

2.4. Fast Fourier Transformed-enhanced IHS (FFT-IHS) –
The basic idea is to modify the input HSR PAN image so that it looks more like the intensity component of the input MS image. Instead of using the total replacement of the intensity component, this method uses a partial replacement based on FFT filtering [5].

1) Transform the MS image from RGB to IHS colour space to obtain the IHS components.
2) Low Pass (LP) filter the intensity component (I) in the Fourier domain.
3) High Pass (HP) filter the PAN image in Fourier domain.
4) Add the high frequency filtered PAN image to the low frequency filtered intensity component, I´.
5) Match I´ to the original I to obtain a new intensity component, I´´.
6) Perform an IHS to RGB transformation on I´´, together with original H and S components to create the fused images.

2.5. Generalised Laplacian Pyramid (GLP) –
The method is a generalisation of the Laplacian pyramid for rational ratio [6]. Two functions are used: the function "reduce" reduces the size of an image of a given q ratio; the function "expand" increases the size of an image of a given p ratio. Degrade an image with a ratio p/q > 1 ("reduce p/q") is done by "expand" by q and "reduce" by p. Interpolate an image can be performed by "expand" by p then "reduce" by q ("expand p/q"). The fusion process is done as follows on each MS image. PAN is decomposed through generalized Laplacian pyramid. The two first levels of Laplacian images are calculated:

$$\begin{cases} \tilde{L}_0 = PAN - expand_{p/q}\left\{reduce_{p/q}(PAN)\right\} \\ \tilde{L}_1 = reduce_{p/q}(PAN) \end{cases} \quad (6)$$

The MS image is interpolated into $MS_{UPGRADE}$ by "expand" by p and "reduce" by q. A coefficient w is calculated from each MS band and $\tilde{L}_1$, $MS_{MERGED} = w * \tilde{L}_0 + MS_{UPGRADE}$ with

$w = \sqrt{var[MS] / var[\tilde{L}_1]}$, where var is the variance calculated for each MS band separately.

2.6.   Local Regression (LR) – The rationale for using a local modelling approach [7] is based on the fact that edges are manifestations of object or material boundaries that occur wherever there is a change in material type, illumination, or topography. The geometrically co-registered PAN band is blurred to match the equivalent resolution of the MS image. A regression analysis within a small moving window (5 x 5) is applied to determine the optimal local modelling coefficients and the residual errors for the pixel neighbourhood using a single MS and the degraded PAN band. Thus,

$$MS_{LOW} = a_{LOW} + b_{LOW} * PAN_{LOW} + e_{LOW.} \quad (7)$$

where, MS_{LOW} is the LSR MS image, a_{LOW} and b_{LOW} are the coefficients, PAN_{LOW} is the degraded LSR PAN band, e_{LOW} is the residual derived from the local regression analysis. Fused image (MS_{HIGH}) is given by:

$$MS_{HIGH} = MS_{LOW} + b_{LOW} * (PAN_{HIGH} - PAN_{LOW}) \quad (8)$$

2.7.   Smoothing Filter (SF) – It is given by:

$$MS_{FUSED} = \frac{MS \times PAN}{PAN_{SMOTHING\_FILTER}} \quad (9)$$

MS is a pixel of LSR image co-registered to HSR PAN band, $PAN_{SMOTHING\_FILTER}$ is average filtered PAN image over a neighbourhood equivalent to the actual resolution of MS image. SF [8] is not applicable for fusing images with different illumination and imaging geometry, such as TM and ESR-1 SAR.

2.8.   Sparkle – Sparkle is a proprietary algorithm developed by the Environmental Research Institute of Michigan (ERIM) [9]. Sparkle treats the digital value of a pixel as being the sum of a low-frequency component and a high-frequency component. It assumes that the low-frequency component is already contained within the MS data and performs two sub-tasks: (1) separate the sharpening image into its low- and high-frequency components, and (2) transfer the high-frequency component to the MS image. The high-frequency component of an area is transferred by multiplying the MS values by the ratio of total sharpening value to its low-frequency component as given by equation (10):

$$MS_{FUSED} = MS^m \times \left(\frac{PAN_{HIGH}}{PAN_{LOW}} \right) \quad (10)$$

where, MS_{FUSED} =fused HSR MS image, MS^m =LSR MS m^{th} band, PAN_{HIGH} =HSR PAN image, $PAN_{LOW} = PAN_{HIGH} *$ h_0, h_0 is a LP filter (average or smoothing filter).

2.9.   SVHC – SVHC (Simulateur de la Vision Humaine des Couleurs) is proposed by CNES, Toulouse France by Marie-Jose Lefevre-Fonollosa [6]. The algorithm is as follows:

1)   Perform a RGB to IHS transformation (IHS_{SVHC} from three MS channels).
2)   Keep H and S images.
3)   Create a low-frequency resolution PAN image ($PAN_{LOW\_FREQUENCY}$), by the suppression of high spatial frequency.
4)   Compute ratio (r), $r = \frac{PAN}{PAN_{LOW}}$.
5)   Compute $I_{MOD} = I \times r$.
6)   Inverse transform from I_{MOD}HS to RGB_{MERGED}.

2.10.   Synthetic Variable Ration (SVR) – It is given by

$$MS_m = PAN_{HIGH} \frac{MS_{HIGH}}{PAN_{HIGH\_SYNTHETIC}} \quad (11)$$

where, MS_m is the grey value of the mth band of the merged HSR IKONOS image, PAN_{HIGH} is the grey value of the original IKONOS PAN image, MS_{HIGH} is the grey value of mth band of IKONOS MS image modified to have the DN as the original IKONOS PAN image, $PAN_{HIGH\_SYTHENTIC}$ is the grey value of the HSR synthetic PAN image simulated through $PAN_{HIGH\_SYNTHETIC} = \sum \varphi_i MS_{HIGH}$. φ_i were calculated directly through multiple regression of the original PAN image and the original MS bands (MS_{HIGH}) which are used in merging and have the same pixel size as PAN_{HIGH} [10].

3.   Data Analysis and Results

Validation of the techniques discussed above was done using IKONOS PAN (spectral wavelength: 525.8 – 928.5 μm, spatial resolution: 1 m, acquired on February 23, 2004) and 4 m spatial resolution MS bands (Blue, Green, Red and Near Infra Red-NIR, acquired on November 24, 2004). The size of PAN and MS images, covering a portion of Bangalore city, India, is 1200 x 1600 and 300 x 400 respectively. The pairs of the images were geometrically registered and the LSR images were upsampled to 1200 x 1600 by nearest neighbour algorithm. IKONOS data were collected at 11-bits per pixel (2048 gray tones). The processing and evaluation were based on the original 11-bit and the data were converted to 8-bit for display purpose only.
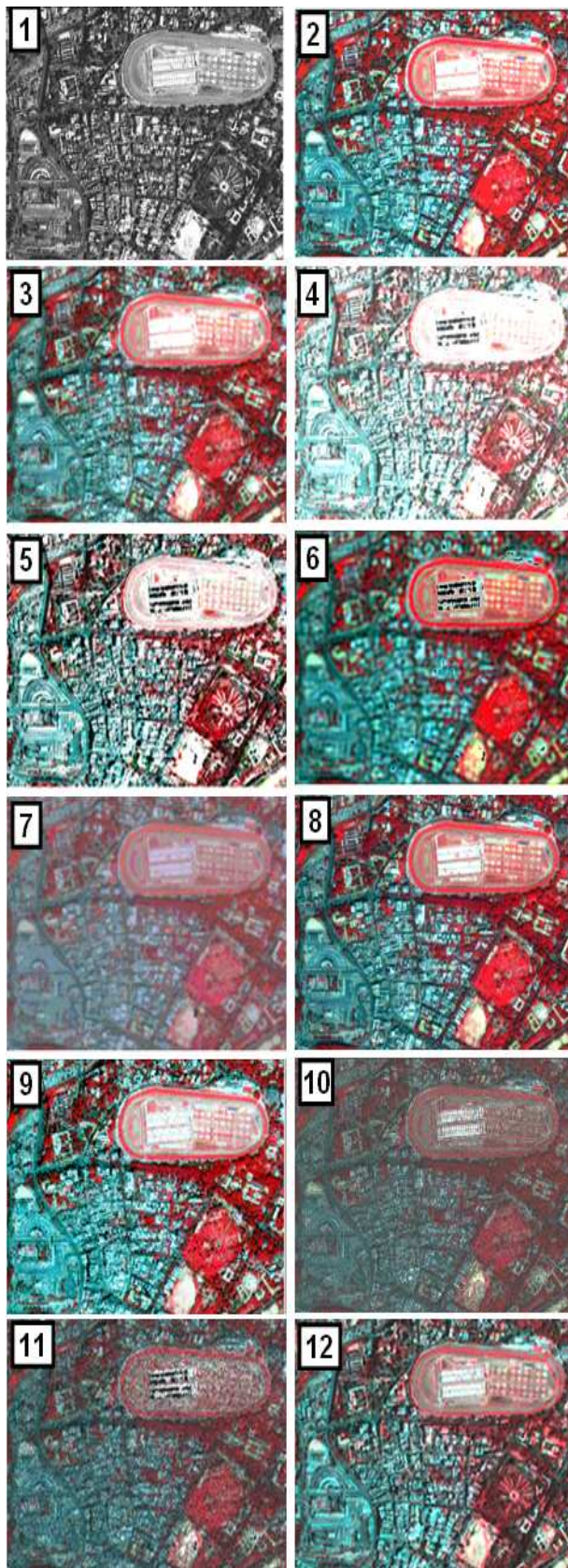
Figure 1. Original PAN image [1], FCC of the original LSR MS image (G-R-NIR) resampled at 1 m pixel size [2], Fusion through COS [3], LMVM [4], Modified IHS [5], FFT-IHS [6], GLP [7], LR [8], SF [9] Sparkle [10], SVHC [11] and SVR [12].

Figure 1 [1 and 2] shows the PAN image and the false colour composite (FCC) of the R-G-B combination resampled at 1 m pixel size. The study area is composed of various features such as buildings, race course, buses, parks, etc. ranging in size from 1 m to 100 m. The correlation coefficients (CCs) between PAN (downsampled to 4 m pixel size) and the original Blue band was 0.41, PAN and Green was 0.44, PAN and Red was 0.47 and PAN and NIR was 0.59. CC of the NIR band is higher than CCs of other bands, indicating that IKONOS NIR band is very important to the IKONOS PAN band. Modified IHS, FFT-IHS and SVHC methods can handle only three bands so G-R-NIR combination was chosen for FCC. The resolution ratio between the IKONOS MS and PAN is 1:4, therefore, in LMVM, FFT-IHS, GLP, LR, SF, Sparkle and SVHC methods, a 5 x 5 filter was used. The regression coefficient $\bar{C}$ in COS between the four MS and PAN band were $C_1=0.19708371$, $C_2=0.80105230$, $C_3=1.355215$ and $C_4=1.3615748$. r was calculated as 0.6633. The modulation coefficient $\bar{W}$ were $W_1=0.3094$, $W_2=0.2944$, $W_3=0.2824$ and $W_4=0.2810$.

The FCC of the G-R-NIR bands (at 1 m) of the fused results of COS, LMVM, Modified IHS, FFT-IHS, GLP, LR, SF, Sparkle, SVHC and SVR methods are displayed in Figure 1 [3-12] respectively. The aim of fusion here is to simulate MS data acquired at LSR (4 m) to HSR level (1 m), which is identical to MS images originally acquired at HSR (1 m), had there been an ideal sensor that would acquire MS bands at 1 m. The performance of the techniques was evaluated in terms of the quality of synthesis of both spatial and spectral information.

Visual inspection indicated that spatial resolutions of the resultant images are higher than that of the original image as features (such as buses, trees, buildings, roads) which were not interpretable in the original image (Figure 1 [2]) are identifiable in the resultant images (Figure 1 [3-12]). LMVM, Modified IHS, GLP and SVHC (Figure 1 [4, 5, 7 and 11]) produce significant color distortion, while FFT-IHS and Sparkle methods (Figure 1 [6 and 10]) produce slight colour distortion in buildings/built-up area. FFT-IHS, GLP and Sparkle exhibit more sharpness. This is probably due to over-enhancement along the edge areas, because these additive methods have considered the differences in high-frequency information between the PAN and the MS bands. Overall, by visual inspection, COS, LR, SF and SVR methods gives the synthesised result closest to what is expected with least colour distortion.

The performance of these techniques were also analysed quantitatively by checking the CC that is often used as a similarity metric in image fusion. However, CC is insensitive to a constant gain and bias between two images and does not allow subtle discrimination of possible fusion artifacts. In addition, a universal image quality index (UIQI) [11 and 12] was used to measure the similarity between two images. UIQI is designed by modeling any image distortion as a combination of three factors: loss of correlation, radiometric distortion, and contrast distortion, and is given by:

$$Q = \frac{\sigma_{AB}}{\sigma_A \sigma_B} \cdot \frac{2\mu_A\mu_B}{\mu_A^2 + \mu_B^2} \cdot \frac{2\sigma_A\sigma_B}{\sigma_A^2 + \sigma_B^2} . \quad (12)$$

The first component is the CC for A (original MS band) and B (fused MS band). The second component measures how close the mean gray levels of A and B is, while the third measures the similarity between the contrasts of A and B. The dynamic range is [-1, 1]. If two images are identical, the similarity is maximal and equals 1. The synthesised HSR MS images (1 m) are spatially degraded to the resolution level of the original LSR MS images (4 m). UIQI are computed between the degraded HSR MS images and the original LSR MS images at the 4 m resolution level. Table 1 shows that the UIQI values of SF and COS are higher than the UIQI values of other methods. SF showed higher scores in the NIR band. Since, PAN band includes the most important information from the NIR band (PAN and NIR exhibited highest correlation), therefore, from the UIQI method, it is apparent that SF and COS are superior to all other methods. CC in Table 1 shows the correlation between the IKONOS HSR PAN image and the corresponding LSR PAN image generated by different methods (computed at 1 m pixel size). It can be seen that the degree of similarity between the HSR PAN image and the LSR PAN image correspond to the degree of spectral distortion of each band. The lower the similarity between the HSR PAN image and the LSR PAN image, the higher the spectral distortion and vice versa. The closeness between original and fused images were also quantified using CC (Table 2) where each original IKONOS MS band was correlated with respect to each fused band obtained from the 10 techniques (except in Modified IHS, FFT-IHS and SVHC where only three bands – G, R, and NIR were considered). SF and COS produced very high correlation of more than 0.9 for all the four bands. GLP has same correlation in all the bands (0.93). LMVM, Modified IHS, FFT-IHS, LR, Sparkle and SVHC produced least correlation. Statistical parameters – minimum, maximum and standard deviation were also used as a measure to examine the spectral information preservation for all the bands (see Figure 2, 3 and 4).

It is evident from Figure 2-4, that LMVM has large deviations from the original band values. COS was closest to original band values for band 1, 2, and 3 while SF was closest to original in band 4 (Figure 2). For the maximum values, (Figure 3), COS and SF fusion methods were very close to the maximum of original bands. All other methods induced changes in the maximum values in all the fused bands. Standard deviation (Figure 4) for SF and COS were closest to original. All other methods showed deviations. While SVR was closer to original band for minimum band values (Figure 2), the technique departed from the original trend for maximum and standard deviation values (Figure 3 and 4). The above statistical parameters indicated that SF and COS are better compared to all other methods, however, it could not clearly indicate which method among SF and COS is better since some values were closer to original bands in SF while some were closer to original band values in COS.

Table 1. UIQI measurements of the similarity between original and the fused images and CC between the HSR PAN and the corresponding PAN image obtained by various methods

Techniques	Blue	Green	Red	NIR	CC
COS	**0.98**	**0.95**	**0.94**	**0.84**	**1.00**
LMVM	0.03	0.05	0.06	0.09	-
Modified IHS	-	0.00	0.00	0.00	**1.00**
FFT-IHS	-	0.42	0.72	0.32	**0.60**
GLP	0.93	0.93	0.93	0.29	-
LR	-0.20	-0.41	-0.40	0.14	-
SF	**0.91**	**0.96**	**0.98**	**0.98**	-
Sparkle	0.04	0.09	0.149	0.12	-
SVHC	-	0.02	0.04	0.06	-
SVR	0.034	0.11	0.23	0.18	**0.32**

- *p* value for all CC = 2.2e⁻¹⁶
- **Modified IHS, FFT-IHS & SVHC are limited to G, R, NIR.**
- **No synthetic PAN in LMVM, GLP, LR, SF, Sparkle & SVHC.**

Table 2. CC between original and fused images

Techniques	Blue	Green	Red	NIR
COS	**0.98**	**0.95**	**0.97**	**0.95**
LMVM	0.04	0.06	0.07	**0.10**
Modified IHS	-	0.09	0.32	**0.18**
FFT-IHS	-	0.20	0.37	**0.29**
GLP	0.93	0.93	0.93	**0.93**
LR	-0.54	-0.58	-0.48	**0.27**
SF	**0.91**	**0.96**	**0.98**	**0.98**
Sparkle	0.11	0.17	0.24	**0.21**
SVHC	-	0.10	0.17	**0.22**
SVR	**0.12**	**0.26**	**0.41**	**0.36**

By combining the visual inspection and the quantitative results, it was observed that, SF has highest UIQI values for Green, Red and NIR bands whereas COS has higher UIQI in Blue band (highlighted in bold in Table 1). The CC values between the HR PAN and LR PAN for COS is 1, while no LR PAN band is generated in SF fusion (Table 1). The CC for SF is higher in bands 2 (Green), 3 (Red) and 4 (NIR) than COS (highlighted in bold in Table 2). Minimum values of band 1 (Blue), 2 (Green), and 3 (Red) are closest to original in COS while SF is closest in band 4 (NIR). Maximum and standard deviation values for all the 4 bands were closest to original in SF than COS. From Table 3, we see that, overall, most of the statistical parameters were closest to original values in band 4 (NIR) for SF (highlighted in Table 3), which is a very important band for IKONOS sensor as it has maximum correlation with the PAN band, so we conclude that SF is better for image fusion.

Table 3. Evaluation of original and fused NIR band by SF and COS methods

	UIQI	CC	Minimum	Maximum	Standard deviation
Original NIR	1.00	1.00	195	811	**87**
SF	**0.98**	**0.98**	**170**	**854**	**88**
COS	**0.84**	**0.95**	**275**	**649**	**52**

There have been a few earlier studies for comparing the efficacy of image fusion algorithms. Z. Wang et al., [11], compared the performance of RGB-IHS, Brovey Transform (BT), High-Pass Filtering (HPF), High-Pass Modulation (HPM), Principal Component Analysis (PCA), À Trous Algorithm-Based Wavelet Transform (ATW) and proposed a new image merging technique – Multiresolution Analysis-Based Intensity Modulation (MRAIM). MRAIM was superior to the other 6 techniques discussed. On the other hand, MRAIM method was inferior to techniques such as High Pass Fusion and ATW, but better than Gram Schmidt (GS) Fusion, CN Spectral, and Luminance Chrominance as communicated in a different study conducted by U. Kumar et al., [12]. Another study by U. Kumar et al., [13] compared the usefulness of RGB-IHS, BT, HPF, HPM, PCA, Fourier Transformation and Correspondence Analysis and showed that HPF was the best among the seven techniques studied. All of the above experiments were conducted on IKONOS 1 m PAN and 4 m MS bands.

Comparison of nine fusion techniques – Multiplicative, BT, RGB-IHS, Pansharp, Local mean matching (LMM), LMVM, Modified IHS, Wavelet and PCA was conducted on QuickBird 0.7 cm PAN and 2.8 m MS images [3], which showed that LMVM, Pansharp and LMM algorithms gathered more advantages for fusion of PAN and MS bands, giving quite good results. However, our work in the current paper proves that SF is much better than LMVM for PAN and MS image fusion. S. Taylor et al., [14] compared BT, Hue Saturation Value, PCA and GS to map Lantana camara. The images were fused and classified into three categories: pasture, forest, and Lantana. Accuracy assessment showed that GS and PCA techniques were best at preserving the spectral information of the original MS image with highest kappa statistic. Another study was carried by A. Svab, [15] to compare IHS, BT and Multiplicative techniques and demonstrated that there is no single method or processing chain for image fusion. A good understanding of the principles of fusing operations, and especially good knowledge of the data characteristics, are compulsory in order to obtain the best results.

M. F. Yakhdani and A. Azizi [16] performed comparative study for IHS, Modified IHS, PCA, Wavelet and BT and found that Modified IHS could preserve the spectral characteristics of the source MS image as well as the HSR characteristics of the source PAN image and are suitable for fusion of IRS P5 and P6 images. In PCA and IHS image fusion, dominant spatial information and weak colour information is a problem, therefore, they should be used for applications such as visual interpretation, image mapping, and photogrammetric purposes. Y. Jinghui et al. [17] performed a general comparison of the pixel level fusion techniques – Component Substitution, Modulation and Multi-resolution Analysis (MRA) based fusion. They concluded that since automatic classification relies on the spectral feature than spatial details, modulation and MRA based techniques with a lower number of decomposition levels are preferable, which better preserve the spectral characteristics of MS bands. For visual interpretation, which benefits from spatial and textural details, CS and MRA techniques with a higher number of decomposition levels are appropriate.

A multi-sensor image fusion for PAN sharpening was done by comparing BT, PCA, Modified IHS, Additive wavelet proportional fusion, GS, Ehlers fusion and University of New Brunswick (UNB) fusion [18]. Various measures of accuracy assessment revealed that standard and most of the advanced fusion methods cannot cope with the demands that are placed on them by multi-sensor/multi-date fusion. The spectral distortions are manifold: brightness reversions, a complete change of spectral characteristics, artificial artifacts or unnatural and artificial colours, etc. Fusion methods such as PC, CN, GS or UNB should only be used for single-sensor, single-date images. Wavelet-based fusions can retain most of the spectral characteristics which comes unfortunately at the expense of spatial improvement. The wavelet method produced additional spatial artifacts instead of spatial improvements. This is probably caused by the wavelet characteristics.

While new methods of image fusion are being developed [19], they should be capable of preserving radiometric and spatial resolutions of the fused data. J. Zhang, [20] reviewed current techniques of multi-source data fusion and discussed their future trends and challenges through the concept of hierarchical classification, i.e., pixel/data level, feature level and decision level using optical PAN and MS data. The selection of an appropriate image fusion method depends on the application. One must use methods that provide suitable results for a defined purpose for better visualization and aids in image interpretation for more accurate mapping, finally improving classification accuracy.

4. Conclusion

This paper reviewed and analysed ten image fusion techniques: COS, LMVM, Modified IHS, FFT-IHS, GLP, LR, SF, Sparkle, SVHC and SVR. The performance of each method was determined by two factors: how the LSR PAN image is computed and how the modulation coefficients are defined. If the LSR PAN image is approximated from the LSR MS image, it usually has a weak correlation with the HSR PAN image, leading to color distortion in the fused image. If the LSR PAN is a LP filtered HSR PAN image, it usually shows less spectral distortion. By combining the visual inspection results and the quantitative results, it is apparent that SF produces the synthesised images closest to those the corresponding multi-sensors would observe at the highest spatial resolution level.
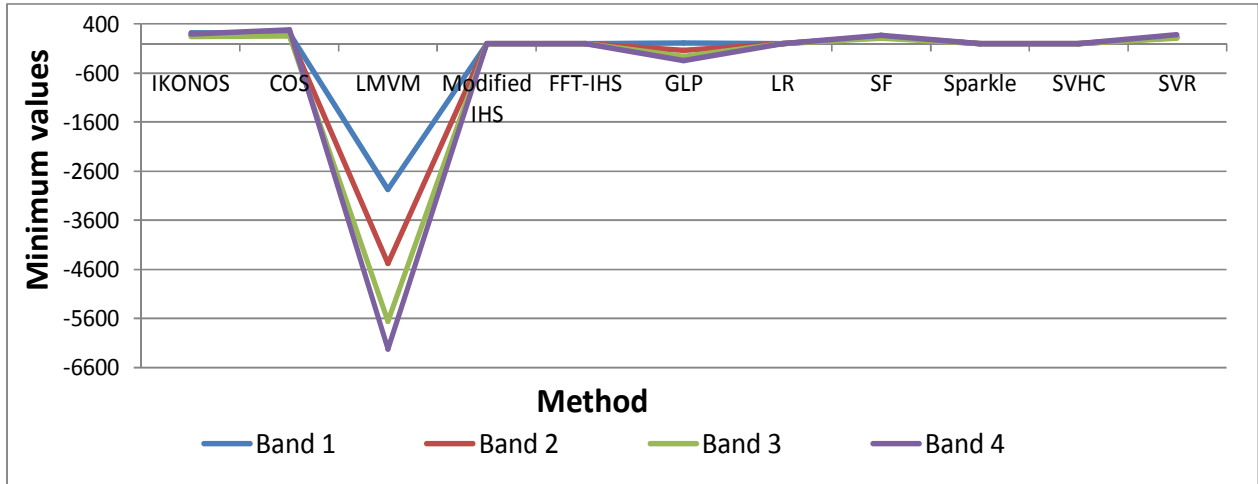
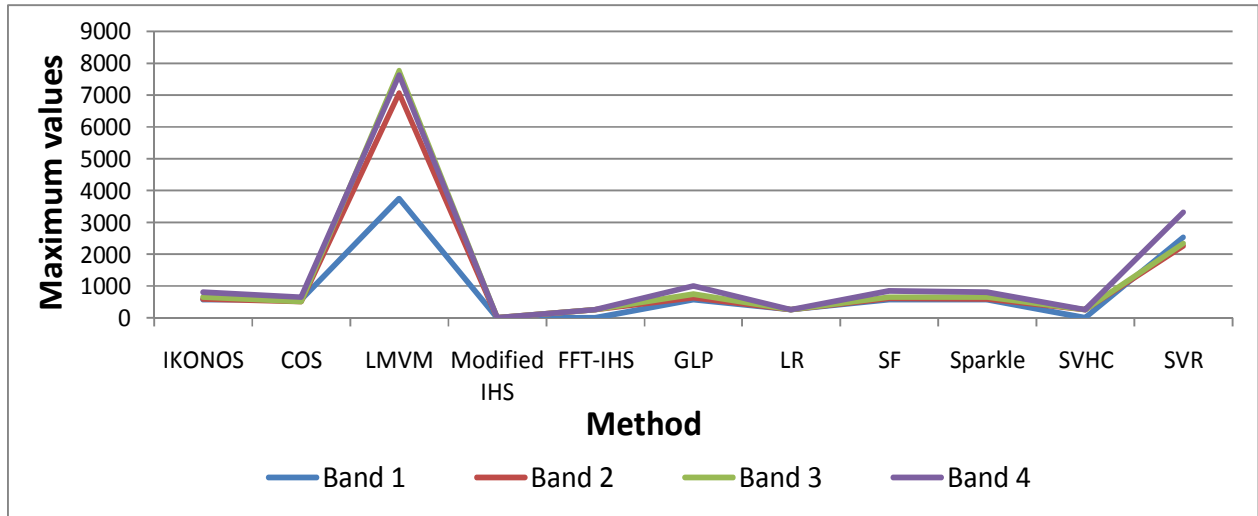**Figure 2.** Minimum values of the original and fused images.
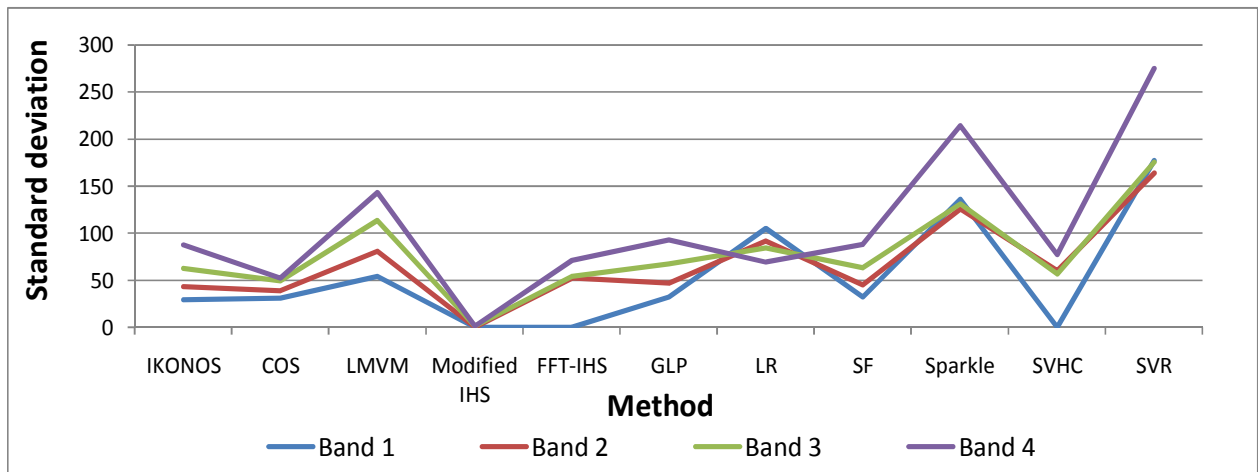

Figure 3. Maximum values of the original and fused images.

Figure 4. Standard deviation values of the original and fused images.

Acknowledgment

References

[1.] H. I. Cakir, and S. Khorram, "Pixel Level Fusion of Panchromatic and Multispectral Images Based on Correspondence Analysis," Photogrammetric Engineering & Remote Sensing, Vol. 74, No. 2, pp. 183-192, 2008.

[2.] W. Dou, Y. Chen, X. Li, D.Z. Sui, "A general framework for component substitution image fusion: An implementation using the fast image fusion method," Computers and Geosciences, Vol. 33, pp. 219-228, 2007.

[3.] K. G. Nikolakopoulos, "Comparison of nine fusion techniques for very high resolution data," Photogrammetry Engineering and Remote Sensing, Vol. 74, No. 5, pp. 647-659, 2008.

[4.] Y. Siddiqui, "The modified IHS method for fusing satellite imagery," In Proceedings of the Annual Conference ASPRS, Anchorage, Alaska, May, 2003.

[5.] Y. Ling, M. Ehlers, E. L. Usery, M Madden, "FFT-enhanced IHS transform method for fusing high-resolution satellite images," ISPRS Journal of Photogrammetry and Remote Sensing, Vol. 61, pp. 381-392, 2007.

[6.] F. Laporterie-Dejean, H. de Boissezon, G. Flouzat, M-J. Lefevre-Fonollosa, "Thematic and statistical evaluation of five panchromatic/multispectral fusion methods on simulated PLEIADES-HR images," Information Fusion, Vol. 6, pp. 193-212, 2005.

[7.] J. Hill, C. Diemer, O. Stover, Th. Udelhoven "A local correlation approach for the fusion of the remote sensing data with different spatial resolutions in forestry applications," International Archieves of Photogrammetry and Remote Sensing, Vol. 32 (7-4-3 W6), 1999.

[8.] J. G. Liu, "Smoothing filter-based intensity modulation: a spectral preserve image fusion technique for improving spatial details," International Journal of Remote Sensing, Vol. 21, No. 18, pp. 3461-3472, 2000.

[9.] J. Vrabel, "Multispectral Imagery Band Sharpening Study," Photogrammetry Engineering and Remote Sensing, Vol. 62, pp. 1075-1083, 1996.

[10.] Y. Zhang, "A new merging method and its spectral and spatial effects," International Journal of Remote Sensing, Vol. 20, No. 10, pp. 2003-2014, 1999.

[11.] Z. Wang, D. Ziou, C. Armenakis, D. Li, and Q. Li, "A Comparative Analysis of Image Fusion Methods," IEEE Transactions of Geoscience and Remote Sensing, Vol. 43, No. 6, pp. 1391-140, 2005.

[12.] U. Kumar, C. Mukhopadhyay, and T. V. Ramachandra, "Pixel based fusion using IKONOS imagery," International Journal of Recent Trends in Engineering (Computer Science), Vol. 1, No. 1, pp. 178-182, 2009.

[13.] U. Kumar, C. Mukhopadhyay and T. V. Ramachandra, "Fusion of Multisensor Data: Review and Comparative Analysis", Proceedings of the 2009 WRI Global Congress on Intelligent Systems, 19-21 May 2009, Xiamen, China, pp. 418 – 422, IEEE Computer Society, Conference Publishing Services, Los Alamitos, California, 2009.

[14.] S. Taylor, L. Kumar, and N. Reid, "Mapping Lantana camara: Accuracy Comparison of Various Fusion Techniques," Photogrammetric Engineering and Remote Sensing, Vol. 76, No. 6, pp. 691-700, 2010

[15.] A. Svab., and K. Ostlr, "High-resolution image Fusion: Methods to Preserve Spectral and Spatial Resolution," Photogrammetric Engineering and Remote Sensing, Vol. 72, No. 5, pp. 565-572, 2006.

[16.] M. F. Yakhdani and A. Azizi "Quality assessment of image fusion techniques for multisensor high resolution satellite images (case study: IRS-P5 and IRS-P6 satellite images)," In: Wagner W., Székely, B. (eds.): ISPRS TC VII Symposium – 100 Years ISPRS, Vienna, Austria, July 5–7, 2010, IAPRS, Vol. XXXVIII, Part 7B.

[17.] Y. Jinghui, Z. Jixian, L. Haitao, S. Yushan, P. Pengxian, "Pixel level fusion methods for remote sensing images: a accurate review," In: Wagner W., Székely, B. (eds.): ISPRS TC VII Symposium – 100 Years ISPRS, Vienna, Austria, July 5–7, 2010, IAPRS, Vol. XXXVIII, Part 7B.

[18.] M. Ehlers, S. Klonusa, P. J. Åstrandb, and P. Rossoa, "Multi-sensor image fusion for pansharpening in remote sensing'," International Journal of Image and Data Fusion, Vol. 1, No. 1, pp. 25-45, 2010.

[19.] B. Yang, and S. Li, "Pixel-level image with simultaneous orthogonal matching pursuit," Information Fusion, 2010. doi:10.1016/j.inffus.2010.04.001

[20.] J. Zhang, "Multi-source remote sensing data fusion: status and trends," International Journal of Image and Data Fusion, Vol. 1, No. 1, pp. 5-24, 2010.